Clinical and Translational Radiation Oncology 18 (2019) 113–119

Contents lists available at ScienceDirect

Clinical and Translational Radiation Oncology

journal homepage: www.elsevier.com/locate/ctro

Original Research Article

Inter-patient variations of radiation-induced normal-tissue changes in Gd-EOB-DTPA-enhanced hepatic MRI scans during fractionated proton therapy

Christian Richter [a,b,c,d,*], Ovidiu C. Andronesi [a,e], Ronald J.H. Borra [a,f,1], Felix Voigt [b], Steffen Löck [b,c,d], Dan G. Duda [a], Alexander R. Guimaraes [a,g,f,2], Theodore S. Hong [a], Thomas R. Bortfeld [a], Joao Seco [a,3]

[a] Department of Radiation Oncology, Massachusetts General Hospital and Harvard Medical School, Boston, MA, USA
[b] OncoRay – National Center for Radiation Research in Oncology, Faculty of Medicine and University Hospital Carl Gustav Carus, Technische Universität Dresden, Dresden, Germany
[c] Department of Radiation Oncology, University Hospital Carl Gustav Carus, Technische Universität Dresden, Dresden, Germany
[d] Helmholtz-Zentrum Dresden – Rossendorf, Institute of Radiooncology – OncoRay, Dresden, Germany
[e] Martinos Center for Biomedical Imaging, Department of Radiology, Massachusetts General Hospital, Boston, MA, USA
[f] Medical Imaging Centre of Southwest Finland, Department of Diagnostic Radiology, Turku University Hospital, Turku, Finland
[g] Division of Abdominal Imaging, Department of Radiology, Massachusetts General Hospital, Boston, MA, USA

ARTICLE INFO

Article history:
Received 19 December 2018
Revised 11 April 2019
Accepted 13 April 2019
Available online 26 April 2019

Keywords:
Gd-EOB-DTPA
Liver
MRI
Radiation-induced changes
Inflammatory response
In vivo verification

ABSTRACT

Background and purpose: Previous MRI studies have shown a substantial decrease in normal-tissue uptake of a hepatobiliary-directed contrast agent 6–9 weeks after liver irradiation. In this prospective clinical study, we investigated whether this effect is detectable during the course of proton therapy.
Material and methods: Gd-EOB-DTPA enhanced MRI was performed twice during hypo-fractionated proton therapy of liver lesions in 9 patients (plus two patients with only one scan available). Dose-correlated signal changes were qualitatively scored based on difference images from the two scans. We evaluated the correlation between the MRI signal change with the planned dose map. The GTV was excluded from all analyses. In addition, were examined timing, irradiated liver volume, changes in liver function parameters as well as circulating biomarkers of inflammation.
Results: Strong, moderate or no dose-correlated signal changes were detected for 2, 3 and 5 patients, respectively. Qualitative scoring was consistent with the quantitative dose to signal change correlation. In an exploratory analysis, the strongest correlation was found between the qualitative scoring and pre-treatment IL-6 concentration. For all patients, a clear dose-correlated signal decrease was seen in late follow-up scans.
Conclusion: Radiation-induced effects can be detected with Gd-EOB-DTPA enhanced MRI in a subgroup of patients within a few days after proton irradiation. The reason for the large inter-patient variations is not yet understood and will require validation in larger studies.

1. Introduction

Range uncertainties can compromise the physical advantage of proton therapy [1–3]. The measurement of the proton range in the patient has been pursued as a means to reduce range uncertainties. Most of those measurement techniques exploit *physical effects*, in particular secondary radiation that is produced by the proton beam, for example through activation of positron emitters, or prompt gamma radiation [4–10].

Biological effects caused by the proton beam have also been used to assess the actual proton range in the patient. An example is the change of the fat content in irradiated bone, which is clearly

* Corresponding author at: OncoRay – National Center for Radiation Research in Oncology, Faculty of Medicine and University Hospital Carl Gustav Carus, Technische Universität Dresden, Dresden, Germany.
E-mail address: christian.richter@oncoray.de (C. Richter).
[1] Current address: Department of Nuclear Medicine and Molecular Imaging, University of Groningen, University Medical Center Groningen, Groningen, the Netherlands.
[2] Current address: Oregon Health & Sciences University, Department of Diagnostic Radiology, Portland, OR, USA.
[3] Current address: Deutsches Krebsforschungszentrum, DKFZ, Division of Biomedical Physics in Radiation Oncology, Heidelberg, Germany.

https://doi.org/10.1016/j.ctro.2019.04.013

visible in MRI scans of the spinal column after proton treatment of medulloblastoma [11]. The advantages of the MRI range assessment method over some of the physics-based methods include the high spatial resolution, the fact that it provides the distal range surface in three dimensions (3-*D*), and that it also provides the anatomical information to correlate the dose information with the patient's anatomy [5]. On the downside, those biological changes typically have been observed late on the MRI images, near or after the completion of the treatment, and they may not be visible at all, certainly not in all disease sites.

We observed changes of the MRI signal in follow up scans acquired 2–3 month after the proton treatment of liver cancer [12]. In particular, the change in the uptake of the hepatocyte-specific contrast media Gd-EOB-DTPA (Eovist, Bayer Schering Pharma, Berlin, Germany) between the irradiated and un-irradiated tissue (as described also for other radiation modalities, see [13–18]) allows for a clear assessment of the proton range. The underlying mechanism appears to be based on (1) radiation-induced cytokine release by Kupffer cells and sinusoidal endothelial cells, (2) activation of inflammatory pathways in the irradiated hepatocytes due to cytokine-mediated signaling, and (3) signaling changes in hepatocytes mainly by transcriptional regulation via nuclear receptors leading to a decrease of the Eovist uptake transporter proteins [19]. In contrast to other Gadolinium-based contrast agents, Gd-EOB-DTPA is actively taken up only by hepatocytes and therefore allowing to assess their functionality.

So far, it remains unclear how long it takes until the effect is MRI-visible in patients, although in vitro data indicated the possibility of a fast reaction within days [20,21]. The purpose of this prospective clinical study was to determine whether the reduced Eovist uptake is detectable already during hypo-fractionated proton irradiation. If the change becomes visible early enough, it could be used to correct any misalignment between the treatment field (in particular the proton range) and the tumor target, and therefore increase the precision of the treatment. It could also provide useful information about the dynamics of the response of the patient to the treatment.

2. Material and methods

2.1. Patients and proton treatment

Eleven patients (40–81 years, median age 62) with intrahepatic metastases were included in this prospective imaging and biomarker study. This study was an IRB-approved embedded optional study of a phase II single-arm clinical trial (NCT01239381). All patients signed informed consent. The primary tumor sites included three rectal, two colon, two pancreatic, one prostate, one breast and one gastric cancer. One patient had a hepatocellular carcinoma. All patients were treated with 3-*D* conformal proton stereotactic body radiotherapy (SBRT) technique, with either 40 Gy (RBE) or 50 Gy (RBE) in 5 fractions over 8–14 days at Massachusetts General Hospital (MGH, Boston, USA). Treatment plans were generated with the commercial treatment planning system XiO (CMS, St. Louis, MO) based on a 4-dimensional computer tomography (CT). The 30% phase of the 4D-CT was selected for treatment planning (in case of gating the 50% phase). Slice thickness was 2.5 mm, and the in-plane spatial resolution was 1.27 mm × 1.27 mm. An additional dual phase helical scan with intravenous contrast was used for target volume delineation. A clinical target volume (CTV) expansion of 0–1 cm around the gross target volume was used. The precise CTV varied based on the confidence of the treating physician to identify the borders of the lesion on imaging. Additional motion and set-up margins of 0.5–1 cm were individually chosen, resulting in the final target volume for passively scattered proton therapy. Patient characteristics, including information about prior chemotherapy and the timing of imaging and therapy, are summarized in Table 1.

2.2. MRI scans

During fractionated proton therapy, two contrast-enhanced MRI scans using T1-weighted inversion recovery (IR) sequences in 3-*D* mode were acquired, usually directly before or after the third and fifth fraction, with the same 1.5 T scanner for all scans and all patients (Siemens Avanto, Siemens Healthcare, Erlangen, Germany). MR images using 3D chemical fat-suppressed T1 weighted gradient-echo volumetric interpolated breath-hold examination axial series with an isotropic voxel size of 2 mm were obtained before and 20 min after intravenous contrast agent injection. For enhanced MRI, 0.025 mmol/kg body weight of Gd-EOB-DTPA was injected though a 20–22 gauge intravenous line (preferably within the antecubital fossa) and injected at 4 cc/sec. To minimize the influence of respiratory motion, the respiration self-navigation mode based on the diaphragm motion was used. Repetition time (TR) was 1550 ms, echo time (TE) was 2.6 ms and inversion time (TI) was 550 ms.

In addition, a T1w gradient echo sequence (VIBE, TR = 2.54 ms, TE = 0.95 ms) and a quantitative T1map sequence with varying flipping angles from 2 to 60° (TR = 8.1 ms, TE = 4.02 ms), both in breath-hold mode were acquired but not used for evaluation. The gradient echo scans possessed in general inferior image quality compared to the navigated scans due to remaining motion. The T1map scans did not cover the whole liver but only 16 slices resulting in inferior image registration results.

2.3. Image registration

To investigate the relationship between radiation dose and MRI signal intensity, the first step was to register the first MRI scan during treatment to the planning CT, upon which the dose calculation was based. In a second step, the second MRI scan was registered to the deformed first MRI scan. For this step, a MRI-MRI registration was favored over a CT-MRI registration due to better registration results and better agreement between both deformed MRI scans. This study excluded pre-treatment MR images because pre-treatment MR images were not available for all the patients.

For both steps, the relevant image volumes were approximately matched by manual alignment to account for the global motion of the liver and then an automated rigid registration followed by a B-spline non-rigid registration was employed to model the local deformation. The registration methods along with the preprocessing step were implemented in the 3D Slicer software [22].

2.4. Evaluation of imaging data

To evaluate dose-correlated signal changes, difference images from the two scans acquired during treatment were calculated. The GTV was excluded from analysis. Before voxelwise subtraction of the signal intensity, both images were normalized to meet the same intensity in the non-irradiated part of the liver. With a median deviation of 8%, the correction was relatively small. Based on the contrast between irradiated and non-irradiated liver, dose-correlated signal changes were qualitatively scored as strong, moderate/weak, or not detectable. The scoring was performed by a single investigator based on the signal difference between irradiated normal liver tissue (in the beam paths) and non-irradiated normal liver tissue (outside the beam paths) in the difference image of the two MRI scans acquired during treatment. Furthermore, the correlation of the detected MRI signal with the planned dose map was analyzed.

Table 1
Patient characteristics including preceding chemotherapy and timing information.

#	Gender	Age [years]	Primary disease site	Dose [Gy]	MRI acquisition	Time between fraction #1 and MRI scan #1 [days]	Time between MRI scans [days]	Time between fraction #1 and follow up MRI [days]	Last chemotherapy Type	Time between last chemo and MRI scan #1
1	F	47	Rectal	50	post3fx, post5fx	5	4	72	FOLFOX	45
2	M	68	HCC	40	post3fx, post5fx	4	5	73	–	–
3	M	40	Rectal	40	post3fx, post5fx	4	6	73	FOLFOX	1523
4	M	81	Gastric	50	post3fx, post5fx	3	5	77	FOLFOX	97
5	F	56	Breast	40	post3fx, post5fx	3	5	84	Xeloda	25
6	F	76	Colon	50	post3fx, post5fx	4	5	122	FLOX + Bevacizumab	850
7	F	62	Pancreas	50	pre5fx	9	–	94	Gemcitabine + Abraxane	51
8	M	66	Colon	50	pre3fx, pre5fx	5	3	75	FOLFOX	1346
9	M	56	Rectal	40	pre4fx	10	–	34	Irinotecan + Cetuximab	70
10	M	81	Prostate	40	pre3fx, pre5fx	7	3	82	Cabazitaxel	102
11	M	58	Pancreas	40	pre3fx, pre5fx	6	3	21	FOLFIRINOX	42

2.5. Evaluation of liver parameters and circulating biomarkers

To evaluate the cause of patient-specific differences in the early response, additional parameters were evaluated: Dose delivered at time of first MRI scan, overall treatment time, time between scans, time between treatment start and first scan, time point and type of preceding chemotherapy, primary disease site, relative irradiated liver volume with $D \geq 5$ Gy, liver function parameters (Aspartate Aminotransferase, Alanine aminotransferase, Bilirubin, Alkaline Phosphatase) and blood (plasma) circulating levels of the cytokines Interleukin (IL)-6, IL-8 and tumor necrosis factor (TNF)-α. Both, liver function and circulating cytokine levels were determined from blood samples taken before and during treatment. Specifically, the relative changes (ratios) of the liver function parameters were analyzed: (a) between pre-treatment (baseline) and second week of treatment; and (b) between week 1 and week 2 of treatment. Moreover, the Prothrombin level at baseline was available. The circulating biomarkers of inflammation were evaluated at baseline and after the 4th fraction of irradiation. Furthermore, the ratio of both values was evaluated. Although the sample size was small, the correlation of these parameters with the qualitative response scoring was tested in a first exploratory analysis using univariate one-way ANOVA with a significance level of 0.05. Statistical analyses were performed using SPSS 23 (IBM Corporation, Armonk, NY, USA).

3. Results

Large inter-patient variations of the radiation-induced changes in Gd-EOB-DTPA enhanced MRI during treatment were found. Strong signal changes during the course of treatment were detected in 2 patients (# 5 and #9), whereas moderate changes were found in 3 patients (#1, #3 and #8). In 5 patients (#2, #4, #6, #10 and #11), we found no dose-correlated early signal change. For one patient (#7) no qualitative scoring of the signal change was possible as only one scan (with no visible dose-correlated signal) was available. Fig. 1 depicts the MRI scans of the patient with the strongest signal change between both scans, and representative MRI scans from patients with moderate or no signal changes are presented in Fig. 2. For one of the two patients with strong dose-correlated signal decrease, the response was already clearly visible in the single MRI scan acquired before the fourth fraction (no second scan was available, see Fig. 3). This was exceptional, because in all other patients no signal decrease in the irradiated area was detectable in the first MRI scan already, but only after evaluating the change between the first and second scan (for the above-mentioned cases of strong and moderate changes). To confirm this visual judgement, we performed a ROI-based evaluation of the irradiated and non-irradiated regions in both scans. We could not find evidence for a signal decrease in the irradiated area at the time of the first scan within the limits of the measurement uncertainties but could confirm the findings of the changes between both scans (cf. Supplement). For all patients a clear dose-correlated signal decrease was seen in late follow up scans (1–4 months post-treatment).

The qualitative scoring was consistent with the quantitative voxelwise dose to signal change correlation (Fig. 4). Patients with a signal change scored as weak or strong showed a clear decrease of MRI signal intensity with increasing dose. In contrast, in patients scored as non-responders, the signal intensity in the difference image was constant or even increasing with increasing dose. The reason for the slight signal increase remained unclear.

As for the additional parameters tested, which could potentially explain inter-patient variations, the strongest correlation was found between early response and pretreatment plasma IL-6 concentration ($p = 0.040$). In the patient group with strong signal change a much higher IL-6 concentration was found compared to the other two groups (5.50 pg/ml vs. 1.44 pg/ml). All other parameters showed no significant differences between the patient groups. The relative irradiated liver volume receiving a dose of at least 5 Gy was higher in the strong responder group than in the moderate responders, however without reaching significance. The values of the evaluated parameters for each qualitative scoring sub-group are presented in Table 2.

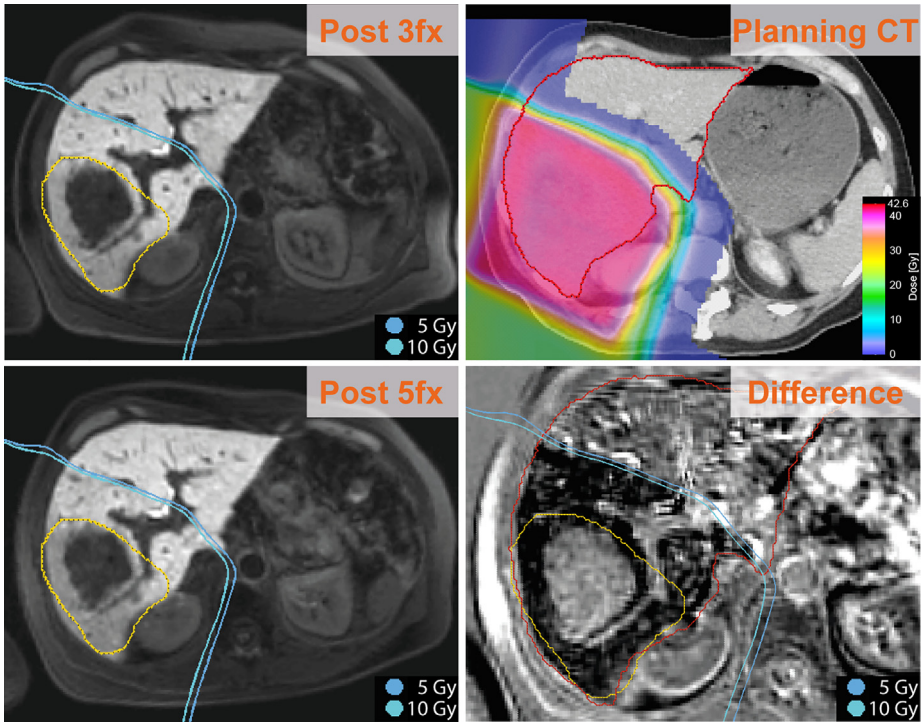

Fig. 1. Patient with strong MRI signal changes (Patient 5): A clear area of decreased Gd-EOB-DTPA uptake is visible in the difference image corresponding to the area treated with doses >5–10 Gy (RBE). The shown 5 Gy and 10 Gy isodose lines were retrieved from the treatment plan. The difference image (lower right corner) was calculated from the two T1-weigthed IR MRI sequences acquired after 3 and 5 fractions, shown on the left. The GTV is represented by the yellow contour. (For interpretation of the references to color in this figure legend, the reader is referred to the web version of this article.)

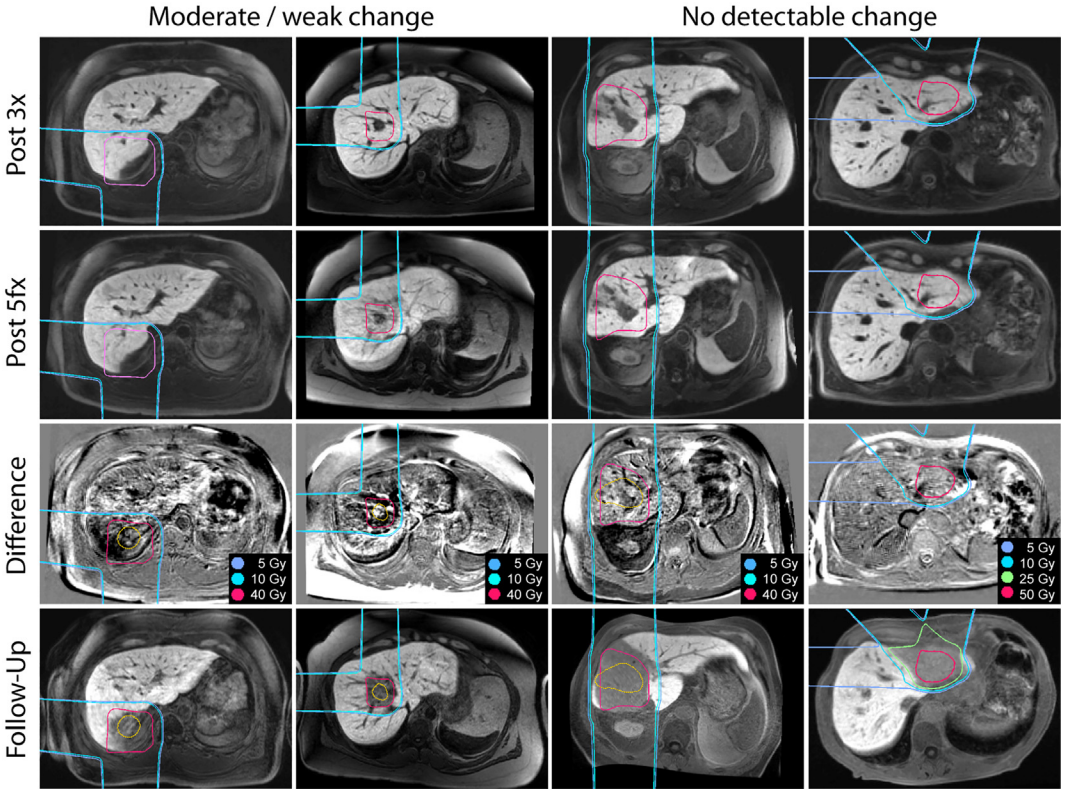

Fig. 2. From left to right, exemplary patients with moderate/weak (Pat. 1 + 3) and no detectable signal change (Pat. 2 + 4) in the difference MRI image (3rd row) of the two scans during therapy (1st and 2nd row). In the difference images, a low signal in the difference image corresponds to a signal decrease in the course of treatment. The GTV is represented by the yellow contour. All cases exhibit a clear signal decrease in follow-up scans (4th row). (For interpretation of the references to color in this figure legend, the reader is referred to the web version of this article.)

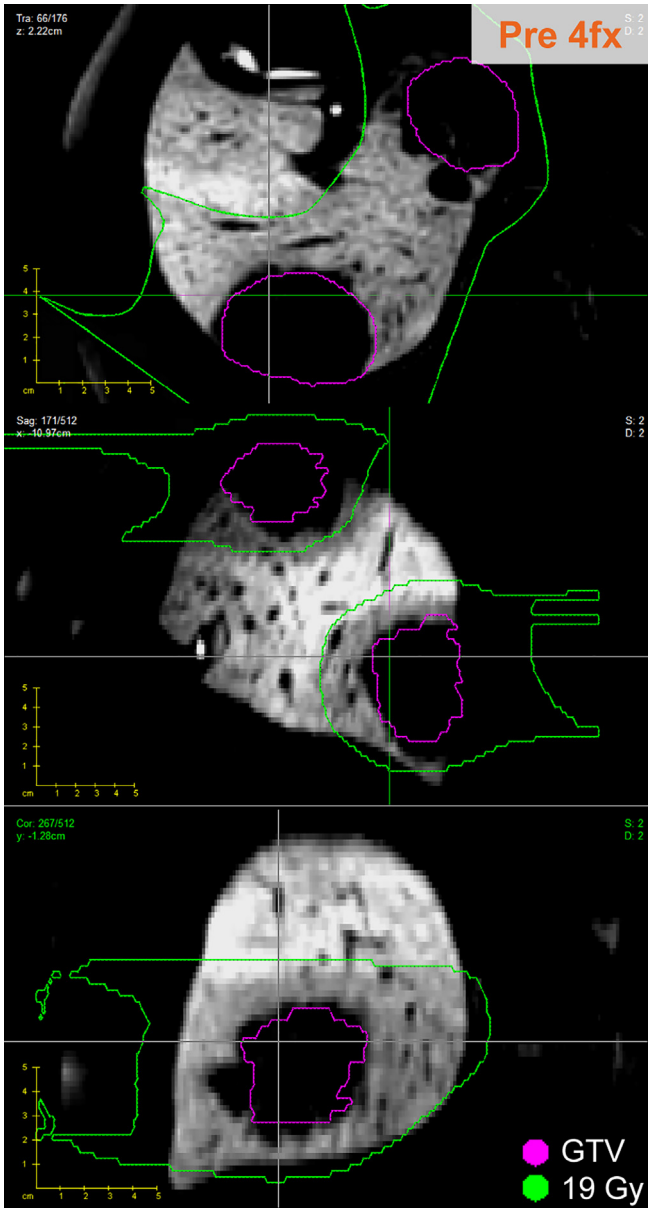

Fig. 3. Axial, coronal and sagital slices of the MRI scan of patient #9 acquired before fraction #4. The purple line outlines the gross tumor volume (GTV) of the liver metastasis showing no Gd-EOB-DTPA uptake. It is surrounded by normal liver tissue with decreased uptake and signal intensity that seems to be in agreement with the area of high dose deposition. (For interpretation of the references to color in this figure legend, the reader is referred to the web version of this article.)

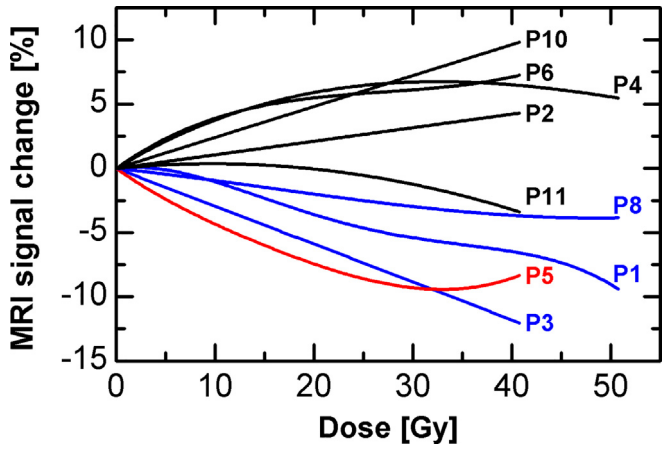

Fig. 4. Quantitative correlation of signal change and planned dose (regression curve for voxelwise correlation) for all patients with two scans during treatment. The color indicates the independent qualitative scoring (red: strong, blue: moderate/weak, black: not detectable). All voxels within the liver, except the GTV, were evaluated. (For interpretation of the references to color in this figure legend, the reader is referred to the web version of this article.)

4. Discussion

We report here for the first time to our knowledge that dose-correlated changes in MRI signal are detectable already during radiation therapy – at least in a subgroup of patients. In contrast to changes seen at late follow-up MRI, which are acquired several weeks after the end of treatment, in the MRI scans during therapy we found large inter-patient variations. These changes ranged from undetectable to very strong signal changes. Although we evaluated liver function parameters and circulating cytokine levels, the underlying causes for these differences between patients are not clear. Moreover, the number of patients included in the presented study was too small to provide clear insights into these heterogeneous responses. Nevertheless, for the two patients with a strong signal change, a high correlation between the position of the area with decreased uptake and the position of the planned dose deposition was found, which is in agreement with the overall uncertainty of the method, e.g., due to image registration. For the patient, where an evaluation of the difference image was possible, the agreement was nearly perfect (cf. Fig. 1), whereas for the other patient (Fig. 3), with only one scan available, there were slight deviations that could possibly be due to registration uncertainty or a slightly different treatment than planned. A recent study from Takamatsu [23], investigating the dose-correlated response after fractionated proton treatment at different time points (end of treatment up to 6 months after treatment), supports our findings of heterogeneous early response: At the end of treatment, in only one of thirteen patients a signal change was found.

Furthermore, our exploratory analyses indicated that the circulating IL-6 level at baseline showed a potential association with the qualitative response scoring and might be a potential biomarker. This might indicate that inflammation at the start of treatment might play a role for the early MRI signal changes. However, the statistical test did not take into account multiple testing and the patient number was limited. Therefore, these hypothesis-generating data should be understood as a first attempt to find a potential explanation for the inter-patient variation in early response and it definitely needs to be further confirmed in larger studies. Other cytokines known to play a role in liver inflammation (e.g., TNF-a or IL-1b) may also be important and should still be included in future blood-based biomarker studies.

One question that was unanswered so far is if the signal change is driven by the amount of deposited dose or mainly by the time duration between irradiation and imaging. From the results, it seems that the irradiation dose does not affect the strength of the signal decrease. Although two different dose levels (40 and 50 GyE) have been used, they revealed no differences in the early or late MRI signal change. Again, the small patient number is a limitation here.

In line with previous studies [15,23], a time-dependence of the so-called threshold dose, the dose necessary to reduce the Gd-EOB-DTPA uptake, was found. It is increasing with increasing time between treatment and MRI scan. Whereas for follow-up scans approximately 2 months after treatment, the threshold dose is between 25 Gy and 40 Gy (cf. also [13]), it is around 5–20 Gy in the scans during treatment for the patients possessing an early response in our study. It should be noted, that this threshold dose

Table 2
Summary of the evaluated parameters separated for the 3 qualitative response groups. For the liver function parameters Δ corresponds to the ratio of the value from week 2 and week 1 after treatment start (Evaluation for the ratio between week 2 and baseline are not shown). For the cytokine parameters Δ corresponds to the ratio of the value from day of the delivery of the 4th fraction and baseline acquisition.

Median (Min-Max)	Qualitative Response scoring		
	0	1	2
Number of patients	5	3	2
Overall treatment time [days]	9 (8–10)	9 (8–10)	11.5 (9–14)
Time between fraction #1 and MRI scan #1 [days]	4 (3–7)	5 (4–5)	6.5 (3–10)
Time between MRI scans [days]	5 (3–5)	4 (3–6)	5 (5–5)
Time between last chemo and MRI scan #1 [days]	100 (0–850)	784 (45–1523)	48 (25–70)
Dose delivered at time of first scan [GyE]	24 (16–30)	24 (20–30)	24 (24–24)
Relative irradiated liver volume with D ≥5 Gy [%]	47 (16–63)	31 (24–37)	61(57–64)
Δ Aspartate Aminotransferase [%]	90 (66–162)	93 (85–96)	101 (96–106)
Δ Alanine aminotransferase [%]	94 (62–207)	95 (88–100)	108 (95–121)
ΔBilirubin [%]	100 (75–100)	100 (67–100)	100 (100–100)
ΔAlbumin [%]	98 (88–100)	96 (93–98)	96 (95–98)
Δ Alkaline Phosphatase [%]	100 (77–147)	98 (89–114)	109 (105–114)
Prothrombin at baseline [s]	13.1 (12.1–31.9)	13.2 (12.5–13.7)	6.7 (1.2–12.1)
IL-6 at baseline [pg/ml]	1.4 (1.2–4.1)	1.6 (0.0–1.7)	5.5 (3.4–7.6)
IL-8 at baseline [pg/ml]	8.4 (2.4–29.6)	4.8 (2.2–23.2)	25.8 (7.2–44.3)
TNF-α at baseline [pg/ml]	2.7 (2.0–3.4)	2.4 (2.0–3.1)	2.4 (1.7–3.1)
ΔIL-6 [%]	174 (93–196)	136 (113–158)	123 (62–184)
ΔIL-8 [%]	122 (89–151)	92 (52–98)	126 (76–176)
ΔTNF-α [%]	86 (71–108)	91 (85–108)	112 (69–155)

of the early response is based only on a subgroup of patients (the ones with detectable MRI signal changes). One could speculate that for the other patients the threshold dose was higher than the delivered dose at that time. Assuming that Gd-EOB-DTPA uptake is correlated to liver functionality as shown in literature [24–26], the temporal development of the threshold dose implicates that it takes longer for the liver tissue to recover from higher doses. Moreover, with growing evidence for a correlation between Gd-EOB-DTPA uptake and liver functionality, the present study also facilitates a better understanding of liver function during the course of proton treatment. Of note, also other methods have been proven to assess liver functionality after radiation therapy, e.g. portal venous perfusion evaluation via CT [27,28] and PET imaging [29]. The study by Fode et al. [29] included that information in treatment plan optimization to reduce dose to highly functional liver regions.

There are some limitations in this study that should be mentioned. First, the number of patients was small. This might be one of the reasons why the cause of the patient variability in early response could not be resolved. Furthermore, no pre-treatment scans using the same imaging protocol were available due to practical reasons. Therefore, only the change during therapy and not the change between pre- and mid-treatment could be analyzed.

Furthermore, a standard, non-quantitative T1-weighted MRI sequence has been used for evaluation. However, extraordinary diligence was used to ensure that scanning conditions were similar between both scans during treatment. The same scanner and scanning protocol was used in all cases. This resulted in very few differences in the absolute MRI signal intensity in the liver between both scans. The remaining differences have been corrected.

Moreover, as a non-rigid image registration was applied to register the MRI scans with the planning CT, the deformation and the resulting voxelwise correlation of MRI signal and dose are associated with unavoidable uncertainties. However, great care was taken including careful visual inspection of each registration result. The registration accuracy was estimated to be within 3 mm, compare also [12] for further evaluation of the registration accuracy of the method used here.

In summary, we report dose-correlated changes in contrast-enhanced MRI scans acquired during radiation therapy. However, due to inter-patient variability in early response, the broad application to *in vivo* verification and adaptation of the dose deposition remains to be established. Nevertheless, further studies should investigate the characteristics and possible reasons for the patient variability in the early phase during irradiation. Eventually, this may become an useful indicator of normal tissue toxicity or therapy outcome. Moreover, we conclude that *in vivo* dose verification using contrast-enhanced MRI in the liver seems to be more robust in late follow-up scans, when a strong MRI signal change with a steep gradient is visible, than during hypo-fractioned therapy.

Conflict of interest

None.

Acknowledgements

This work was supported in part by NCI Federal Share Program funding (C06-CA059267: Proton Therapy Research and Treatment Center to T.R.B., and an Independent Grant to D.G.D.). C.R. is supported by the German Federal Ministry of Education and Research (BMBF-03Z1N51). For clarification: CR was working at MGH (USA) as visiting scientist when the study was initiated. During evaluation CR was working at OncoRay (Germany). T.S.H. was supported in part by funding from the Cancer Clinical Investigator Team Leadership Award awarded by the NCI though a supplement to P30CA006516. D.G.D. was supported by the NCI grant P01-CA80124.

Appendix A. Supplementary data

Supplementary data to this article can be found online at https://doi.org/10.1016/j.ctro.2019.04.013.

References

[1] Paganetti H. Range uncertainties in proton therapy and the role of Monte Carlo simulations. Phys Med Biol 2012;57:117.
[2] Yang M, Zhu XR, Park PC, et al. Comprehensive analysis of proton range uncertainties related to patient stopping-power-ratio estimation using the stoichiometric calibration. Phys Med Biol 2012;57:4095–115.
[3] Lomax AJ, Boehringer T, Coray A, et al. Intensity modulated proton therapy. A clinical example. Med Phys 2001;28:317.

[4] Parodi K, Paganetti H, Shih HA, et al. Patient study of in vivo verification of beam delivery and range, using positron emission tomography and computed tomography imaging after proton therapy. Int J Radiat Oncol Biol Phys 2007;68:920–34.
[5] Knopf A-C, Lomax A. In vivo proton range verification: a review. Phys Med Biol 2013;58:60.
[6] Enghardt W, Parodi K, Crespo P, Fiedler F, Pawelke J, Pönisch F. Dose quantification from in-beam positron emission tomography. Radiother Oncol 2004;73:S96–8.
[7] Shakirin G, Braess H, Fiedler F, et al. Implementation and workflow for PET monitoring of therapeutic ion irradiation: a comparison of in-beam, in-room, and off-line techniques. Phys Med Biol 2011;56:1281–98.
[8] Smeets J, Roellinghoff F, Prieels D, et al. Prompt gamma imaging with a slit camera for real-time range control in proton therapy. Phys Med Biol 2012;57:3371–405.
[9] Verburg JM, Riley K, Bortfeld T, Seco J. Energy- and time-resolved detection of prompt gamma-rays for proton range verification. Phys Med Biol 2013;58:49.
[10] Golnik C, Hueso-González F, Müller A, et al. Range assessment in particle therapy based on prompt γ-ray timing measurements. Phys Med Biol 2014;59:5399–422.
[11] Gensheimer MF, Yock TI, Liebsch NJ, et al. In Vivo Proton Beam Range Verification Using Spine MRI Changes. Int J Radiat Oncol Biol Phys 2010;78:268–75.
[12] Yuan Y, Andronesi O, Bortfeld T, Guimaraes A, Hong T, Seco J. Feasibility study of MRI in assessing in vivo proton end-of-range for liver cancer. Med. Phys 2011;38:3743.
[13] Sanuki N, Takeda A, Oku Y, et al. Threshold doses for focal liver reaction after stereotactic ablative body radiation therapy for small hepatocellular carcinoma depend on liver function: evaluation on magnetic resonance imaging With Gd-EOB-DTPA. Int J Radiat Oncol Biol Phys 2014;88:306–11.
[14] Seidensticker M, Seidensticker R, Mohnike K, et al. Quantitative in vivo assessment of radiation injury of the liver using Gd-EOB-DTPA enhanced MRI: tolerance dose of small liver volumes. Radiat Oncol 2011;6:40.
[15] Seidensticker M, Burak M, Kalinski T, et al. Radiation-induced liver damage: correlation of histopathology with hepatobiliary magnetic resonance imaging, a feasibility study. Cardiovasc Intervent Radiol 2015;38:213–21.
[16] Wybranski C, Eberhardt B, Fischbach K, et al. Accuracy of applicator tip reconstruction in MRI-guided interstitial (192)Ir-high-dose-rate brachytherapy of liver tumors. Radiother Oncol 2015;115:72–7.
[17] Jung J, Yoon SM, Cho B, et al. Hepatic reaction dose for parenchymal changes on Gd-EOB-DTPA-enhanced magnetic resonance images after stereotactic body radiation therapy for hepatocellular carcinoma. J Med Imag Radiat Oncol 2016;60:96–101.
[18] Doi H, Shiomi H, Masai N, et al. Threshold doses and prediction of visually apparent liver dysfunction after stereotactic body radiation therapy in cirrhotic and normal livers using magnetic resonance imaging. J Radiat Res 2016;57:294–300.
[19] Richter C, Seco J, Hong TS, Duda DG, Bortfeld T. Radiation-induced changes in hepatocyte-specific Gd-EOB-DTPA enhanced MRI: potential mechanism. Med Hypotheses 2014;83:477–81.
[20] Le Vee M, Lecureur V, Stieger B, Fardel O. Regulation of drug transporter expression in human hepatocytes exposed to the proinflammatory cytokines tumor necrosis factor-alpha or interleukin-6. Drug Metab Dispos 2009;37:685–93.
[21] Fardel O, Le Vée M. Regulation of human hepatic drug transporter expression by pro-inflammatory cytokines. Expert Opin Drug Metab Toxicol 2009;5:1469–81.
[22] Fedorov A, Beichel R, Kalpathy-Cramer J, et al. 3D Slicer as an image computing platform for the Quantitative Imaging Network. Magn Reson Imaging 2012;30:1323–41.
[23] Takamatsu S, Yamamoto K, Maeda Y, et al. Evaluation of focal liver reaction after proton beam therapy for hepatocellular carcinoma examined using Gd-EOB-DTPA enhanced hepatic magnetic resonance imaging. PLoS One 2016;11:e0167155.
[24] Verloh N, Haimerl M, Zeman F, et al. Assessing liver function by liver enhancement during the hepatobiliary phase with Gd-EOB-DTPA-enhanced MRI at 3 Tesla. Eur Radiol 2014;24:1013–9.
[25] Talakic E, Steiner J, Kalmar P, et al. Gd-EOB-DTPA enhanced MRI of the liver: correlation of relative hepatic enhancement, relative renal enhancement, and liver to kidneys enhancement ratio with serum hepatic enzyme levels and eGFR. Eur J Radiol 2014;83:607–11.
[26] Utsunomiya T, Shimada M, Hanaoka J, et al. Possible utility of MRI using Gd-EOB-DTPA for estimating liver functional reserve. J Gastroenterol 2012;47:470–6.
[27] Cao Y, Wang H, Johnson TD, et al. Prediction of liver function by using magnetic resonance-based portal venous perfusion imaging. Int. J. Radiat. Oncol. Biol. Phys. 2013;85:258–63.
[28] Cao Y, Pan C, Balter JM, et al. Liver function after irradiation based on computed tomographic portal vein perfusion imaging. Int J Radiat Oncol Biol Phys 2008;70:154–60.
[29] Fode MM, Petersen JB, Sørensen M, Holt MI, Keiding S, Høyer M. 2-[18 F]fluoro-2-deoxy- d -galactose positron emission tomography guided functional treatment planning of stereotactic body radiotherapy of liver tumours. Phys Imag Radiat Oncol 2017;1:28–33.